Disruption of Cxcr3 chemotactic signaling alters lysosomal function and renders macrophages more microbicidal

Sommer, F.; Torraca, V.; Xie, Y.; Veld, A.E. in 't; Willemse, J.J.; Meijer, A.H.

Cell Reports

Report

Disruption of Cxcr3 chemotactic signaling alters lysosomal function and renders macrophages more microbicidal

Graphical abstract

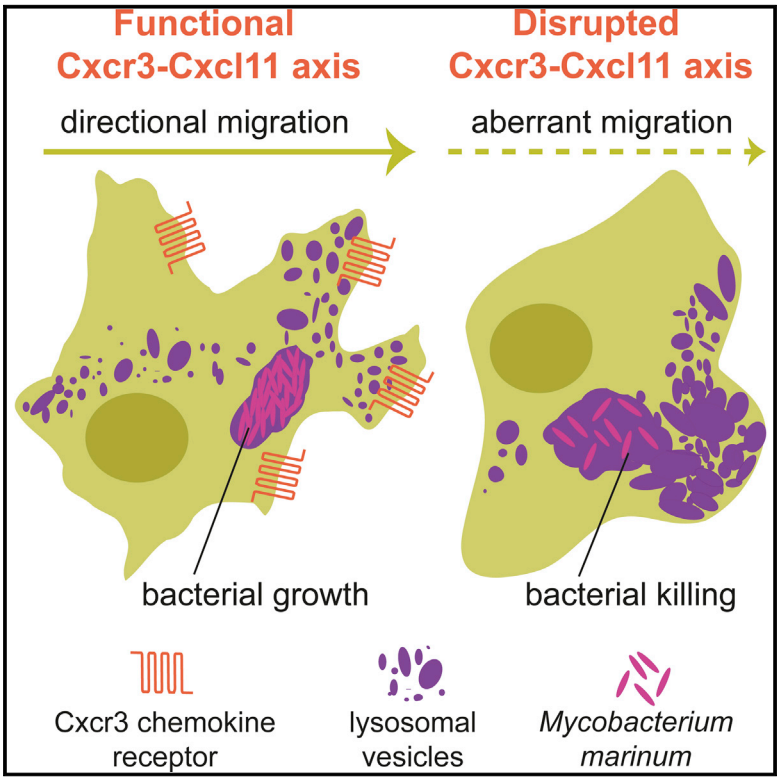

Authors

Frida Sommer, Vincenzo Torraca, Yufei Xie, Aliede E. in 't Veld, Joost Willemse, Annemarie H. Meijer

Correspondence

a.h.meijer@biology.leidenuniv.nl

In brief

Sommer et al. show that migration of immune cells is inversely linked to their bactericidal properties. Disrupting Cxcr3 chemotactic signaling affects lysosome trafficking and augments lysosomal capacity. Consequently, while reducing migration, Cxcr3 deficiency also primes immune cells for better clearance of intracellular infection.

Highlights

- Disruption of Cxcr3 chemotactic signaling increases lysosomal gene expression
- Cxcr3 deficiency augments the microbicidal capacity of macrophages
- The lysosomal regulator TFEC counteracts the effect of Cxcr3 on microbicidal capacity
- Cxcr3 deficiency affects lysosome trafficking and prevents polarized migration

Sommer et al., 2021, Cell Reports *35*, 109000
April 13, 2021
https://doi.org/10.1016/j.celrep.2021.109000

CellPress

Cell Reports

CellPress
OPEN ACCESS

Report

Disruption of Cxcr3 chemotactic signaling alters lysosomal function and renders macrophages more microbicidal

Frida Sommer,[1] Vincenzo Torraca,[1,2] Yufei Xie,[1] Aliede E. in 't Veld,[1] Joost Willemse,[1] and Annemarie H. Meijer[1,3,*]
[1]Institute of Biology Leiden, Leiden University, Leiden, the Netherlands
[2]Department of Infection Biology, London School of Hygiene & Tropical Medicine, London, UK
[3]Lead contact
*Correspondence: a.h.meijer@biology.leidenuniv.nl
https://doi.org/10.1016/j.celrep.2021.109000

SUMMARY

Chemotaxis and lysosomal function are closely intertwined processes essential for the inflammatory response and clearance of intracellular bacteria. We used the zebrafish model to examine the link between chemotactic signaling and lysosome physiology in macrophages during mycobacterial infection and wound-induced inflammation *in vivo*. Macrophages from zebrafish larvae carrying a mutation in a chemokine receptor of the Cxcr3 family display upregulated expression of vesicle trafficking and lysosomal genes and possess enlarged lysosomes that enhance intracellular bacterial clearance. This increased microbicidal capacity is phenocopied by inhibiting the lysosomal transcription factor EC, while its overexpression counteracts the protective effect of chemokine receptor mutation. Tracking macrophage migration in zebrafish revealed that lysosomes of chemokine receptor mutants accumulate in the front half of cells, preventing macrophage polarization during chemotaxis and reaching sites of inflammation. Our work shows that chemotactic signaling affects the bactericidal properties and localization during chemotaxis, key aspects of the inflammatory response.

INTRODUCTION

Macrophages are specialized motile cells that mediate the innate immune response to pathogens, initiate inflammation, present antigens, regulate tissue repair, and also have diverse functions in developmental processes (Ginhoux et al., 2016). Similar to other leukocytes, macrophages differentially express chemokine receptors to sense extracellular cues that direct them to inflammatory sites (Charo and Ransohoff, 2006; Rot and von Andrian, 2004). Following chemotactic stimulation, these cells acquire a polarized phenotype characterized by clearly identifiable lamellipodia (leading edge) and a uropod (rear edge) that involves both the contractile machinery of the cell and the intracellular vesicle trafficking system (Colvin et al., 2010). Recent studies revealed that intracellular vesicular trafficking, particularly lysosomes and the secretion of exosomes, plays a role in regulating chemotaxis (Colvin et al., 2010; Sung et al., 2015; Bretou et al., 2017; Becker, 1976; del Pozo et al., 1995; Reddy et al., 2001). The Ca^{2+} release triggered by chemokine receptors induces the fusion of lysosomes with the plasma membrane at the uropod to sustain cell shape remodeling through the delivery of endomembranes and to detach the uropod (Colvin et al., 2010; del Pozo et al., 1995; Bretou et al., 2017; Becker 1976; Reddy et al., 2001; Lawson and Maxfield, 1995). Synaptotagmins (calcium-sensing vesicle-fusion proteins) and Rab GTPases are critical regulators of vesicular trafficking and lysosomal exocytosis and link the chemokine signaling-dependent Ca^{2+} flux to lysosomal function (Colvin et al., 2010; Constantin and Laudanna, 2010; Lawson and Maxfield, 1995; Colvin and Luster, 2011). Processes linking cell motility and lysosomal function are only partially understood, and the effect of chemokine signaling on lysosomal function during inflammatory processes *in vivo* remains largely unknown.

Lysosomes are acidic membrane-bound organelles, rich in hydrolytic enzymes that mediate the catabolism of various macromolecules (Luzio et al., 2014; De Duve et al., 1955). In addition to their function as digestive organelles, lysosomes have emerged as signaling platforms and as critical regulators of cell metabolism, homeostasis, plasma membrane repair, survival, and immune defense (Martina et al., 2014; Settembre et al., 2013; Lawrence and Zoncu 2019; Zoncu et al., 2011). The mammalian/mechanistic target of rapamycin complex 1 (mTORC1), a kinase complex anchored to the lysosomal membrane, is a key regulator of lysosomal function (Martina et al., 2012; Settembre et al., 2012). The serine/threonine kinase mTOR phosphorylates the master gene of lysosomal biogenesis TFEB (transcription factor EB) to prevent its translocation to the nucleus (Sardiello et al., 2009; Palmieri et al., 2011; Verastegui et al., 2000). TFEB is a member of the basic helix-loop-helix leucine zipper family of transcription factors that bind to the CLEAR (coordinated lysosomal expression and regulation) elements (GTCACGTGAC) in the promoter regions of autophagic and lysosomal genes

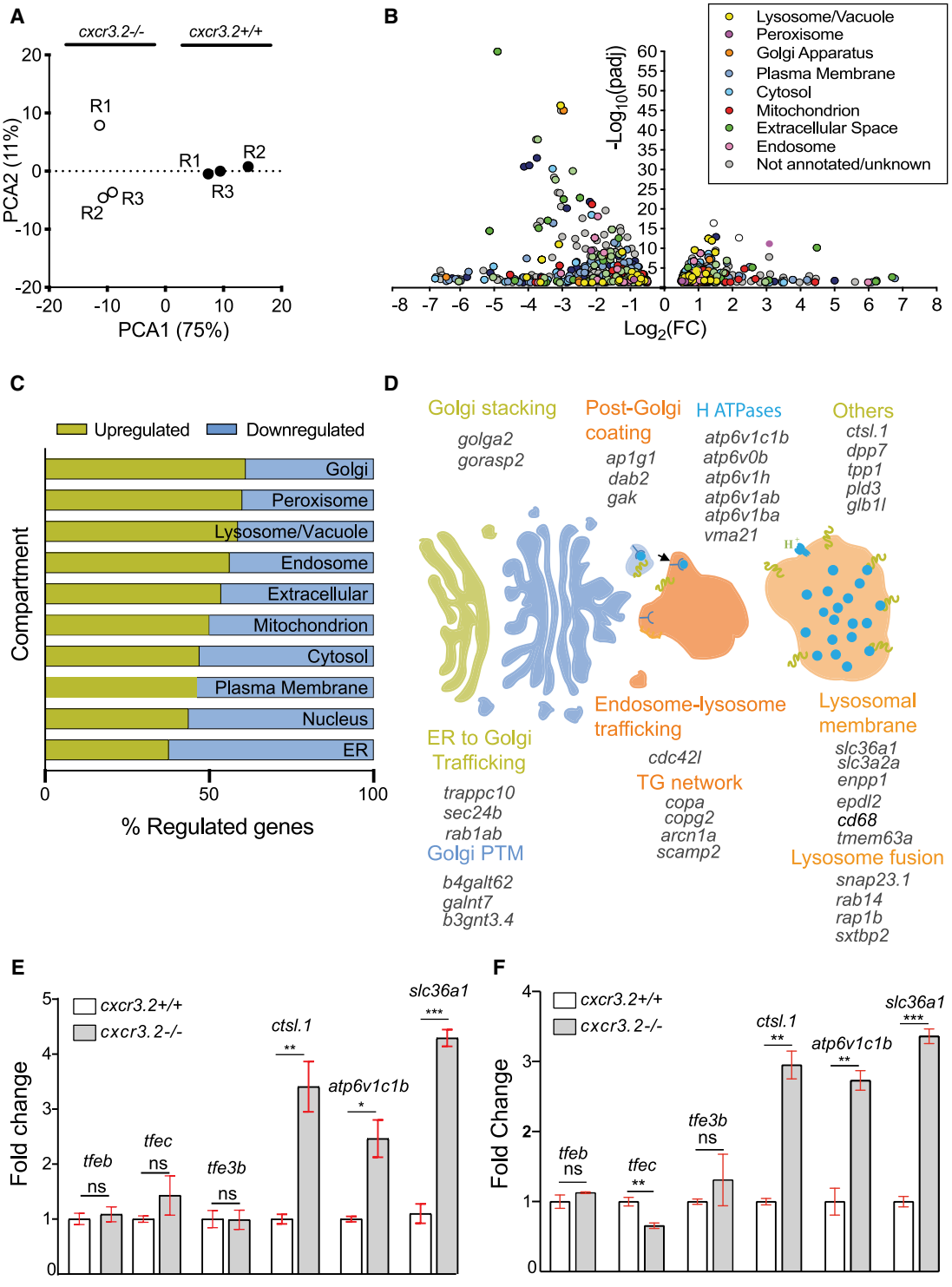

Figure 1. Disruption of Cxcr3.2 signaling transcriptionally induces genes related to lysosomal function and intracellular vesicle trafficking

(A) Principal-component analysis (PCA) of *cxcr3.2* mutant (*cxcr3.2*$^{-/-}$) and WT (*cxcr3.2*$^{+/+}$) transcriptomes. PCA analysis was performed in R on variance-stabilizing transformed (vst) data, using the DESeq2 plotPCA command.

(B) Volcano plot of *cxcr3.2* mutant versus WT differentially expressed genes. Genes are classified and color-coded by cellular compartment annotation. Compartment annotations were obtained from http://geneontology.org according to the GO cellular component and from KEGG pathways.

(C) Distribution of upregulated (yellow) and downregulated (blue) genes, classified by compartment as above. Lysosomal, Golgi, and peroxisome-related genes are more commonly upregulated in *cxcr3.2* mutant macrophages.

(legend continued on next page)

(Sardiello et al., 2009; Palmieri et al., 2011). It belongs to the microphthalmia-associated transcription factor and TFE (MiTF/TFE) family, which also includes TFEC (transcription factor EC), TFE3 (transcription factor E3), and MITF (melanocyte inducing transcription factor) (Sardiello et al., 2009; Verastegui et al., 2000; Pastore et al., 2019). TFE3 dimers or TFE3-TFEB heterodimers cooperatively orchestrate lysosomal biogenesis and exocytosis by binding to overlapping sets of CLEAR elements (Pastore et al., 2017; Raben and Puertollano, 2016). However, the involvement of TFEC in lysosomal function remains elusive (Mahony et al., 2016; Lister et al., 2011). Early reports suggest that TFEC acts as a repressor of lysosomal biogenesis (Zhao et al., 1993; Steingrímsson et al., 2002). It was later suggested that different isoforms of TFEC can enhance lysosomal biogenesis in a cell-specific manner; therefore, TFEC is now ascribed mostly a dual role (Chung et al., 2001; Yasumoto and Shibahara, 1997).

In macrophages, lysosomes are involved in pro-inflammatory, chemoattractant, and antimicrobial responses (Bretou et al., 2017; Settembre et al., 2013; Pastore et al., 2016; Visvikis et al., 2014). Following their phagocytic uptake by macrophages, microbes are enclosed inside a phagosome, which gradually matures by acquiring lysosomal hydrolases, a process that goes along with acidification and production of antimicrobial molecules (Sachdeva and Sundaramurthy, 2020). However, a number of intracellular pathogens, with *Mycobacterium tuberculosis* as a notable example, are able to inhibit phagosome maturation and avoid lysosomal degradation (Upadhyay et al., 2018; Flannagan et al., 2015; Tuli and Sharma, 2019). Macrophage recognition of pathogen- and damage-associated molecular patterns (PAMPs and DAMPs) primes lysosomes for pathogen degradation and chemotaxis in an mTORC1-independent manner (Bretou et al., 2017; Shen et al., 2016; El-Houjeiri et al., 2019). Pathogen sensing through Toll-like receptors (TLRs) triggers the release of calcium from the lysosome through the MCOLIN 1 (mucolipin 1) ion channel and activates calcineurin, which dephosphorylates TFEB and facilitates its translocation to the nucleus (Bretou et al., 2017; Medina et al., 2015; Tong and Song, 2015; Schilling et al., 2013). TFEB activation leads to increased phagosomal acidification and accumulation of lysosomes (Settembre et al., 2013; El-Houjeiri et al., 2019; Settembre et al., 2011). Likewise, macrophages activated by TLR sensing show accumulation of TFE3 in the nucleus and induction of immune genes directly implicated in the inflammatory response (Pastore et al., 2016; Schilling et al., 2013). In contrast, depletion of TFEB or TFE3 results in reduced cytokine and chemokine secretion (Pastore et al., 2016; Visvikis et al., 2014; Settembre et al., 2011). Thus, the function of the lysosomal transcriptional regulators is tightly linked to macrophage migration.

In the present study, we investigated the link between chemotactic signaling and lysosomal function *in vivo* using a *cxcr3.2* mutant zebrafish line deficient in a macrophage-attractant chemokine receptor homologous to human CXCR3 (Torraca et al., 2015). We previously showed that zebrafish larvae lacking Cxcr3.2 are more resistant to mycobacterial infection and that reduced motility of macrophages limits the tissue dissemination of mycobacteria (Torraca et al., 2015; Sommer et al., 2020). In this study, we report that RNA deep sequencing (RNA-seq) data of these macrophages revealed a dysregulation of lysosomal and Golgi-related genes. In agreement, we found that chemokine signaling disruption in macrophages was linked to increased lysosomal staining and enhanced clearance of a mycobacterial pathogen. Supporting the connection between Cxcr3 chemotactic signaling and lysosomal function, we found that expression of dominant-negative Tfec phenocopied the infection resistance of *cxcr3.2* mutants, while their enhanced microbicidal capacity was counteracted by *tfec* overexpression. Finally, we assessed whether aberrant macrophage motility in *cxcr3.2* mutants was linked to altered subcellular lysosome dynamics during chemotaxis. Indeed, we observed that cell polarization in mutant macrophages was incomplete, with lysosomes failing to shuttle between the leading and trailing edges of the cell. Taken together, these results link macrophage chemotaxis to intracellular vesicular trafficking, showing that disruption of the Cxcr3 axis induces lysosomal gene expression and renders macrophages more microbicidal against intracellular bacteria.

RESULTS

Intracellular vesicle trafficking and lysosomal genes are upregulated when Cxcr3.2 chemotactic signaling is disrupted

The zebrafish Cxcr3.2 chemokine receptor is a functional homolog of human CXCR3. In developing zebrafish larvae lacking the Cxcr3.2 receptor, we observed that the macrophages display reduced random motility compared to macrophages in wild-type (WT) larvae (Torraca et al., 2015). In addition, Cxcr3.2-deficient macrophages are impaired in directed migration to the receptor ligand (Cxcl11aa) and to sites of infection and injury where the production of this chemokine is increased (Torraca et al., 2015; Sommer et al., 2020; Xie et al., 2019). To identify genes and biological pathways affected by the disruption of Cxcr3 signaling, we sorted macrophages from *cxcr3.2* mutant and WT zebrafish larvae under non-infected conditions and subjected these to RNA-seq. Principal-component analysis (PCA) confirmed overall distinction between the *cxcr3.2* mutant and WT transcriptomic profiles (Figure 1A). Differential expression analysis revealed that *cxcr3.2* mutation led to the

(D) Graphical representation of induced genes exerting key functions in Golgi and lysosomal pathways. ER, endoplasmic reticulum; PTM, post-translational modification; TG, *trans*-Golgi.

(E and F) Expression fold change of representative lysosomal markers and transcriptional regulators of lysosomal functions of *cxcr3.2* mutant and WT FACS macrophages, as determined by qPCR (E) or RNA-seq analysis (F). qPCR analysis confirmed that overall lysosomal function is increased in *cxcr3.2* mutants as indicated by the upregulation of lysosomal function markers *ctsl.1*, *atp6v1c1b*, and *slc36a1*, whereas the expression of the lysosomal biogenesis regulators *tfeb*, *tfe3*, and *tfec* remained unaltered. Three biological samples of 150–200 larvae were used, and three technical replicates were conducted. Data were analyzed using a two-tailed t test and results are shown as mean ± SEM (*$p \leq 0.05$, **$p \leq 0.01$, ***$p \leq 0.001$; ns, not significant [$p > 0.05$]).

downregulation of 490 genes and upregulation of 407 genes (Data S1) among different subcellular compartments (Figure 1B; Data 2). Classification of these genes by compartment showed that peroxisomal, lysosomal, and Golgi-related genes were most frequently upregulated (Figure 1C; Data S2), although only lysosomal- and Golgi-related terms were significantly differentially represented in Gene Ontology (GO) or Kyoto Encyclopedia of Genes and Genomes (KEGG) enrichment analysis, i.e., KEGG "lysosome," GO cellular components "Golgi-associated vesicle," "Golgi apparatus," "ER-Golgi intermediate compartment," "lysosome," "vacuole," and GO biological process "Golgi vesicle transport" (Data S3). Differentially expressed genes related to lysosomal and Golgi function were also classified under different processes, including Golgi stacking, post-Golgi coating, endoplasmic reticulum (ER) to Golgi trafficking, Golgi post-translational modifications (Golgi-PTM), endosome-lysosome trafficking, *trans*-Golgi network (TGN) function, lysosomal biogenesis and maturation, and proton transport (Figure 1D). To confirm the upregulation of lysosomal genes, we ran a qPCR on marker genes *ctsl.1* (lysosomal cysteine protease), *atp6v1c1b* (acidifies intracellular compartments), and *slc36a1* (lysosomal amino acid transporter) and lysosomal regulators *tfeb*, *tfe3,* and *tfec*. All lysosomal markers showed upregulation comparable to those observed in the RNA-seq profile (Figures 1E and 1F). However, the expression of the lysosomal regulators was unaffected, indicating that the effects on lysosomal gene expression cannot be attributed to changes in the transcription of *tfeb*, *tfe3b*, or *tfec*. Collectively, our data suggest that disruption of the Cxcr3 axis induces a transcriptional increase in genes related to lysosomal function and intracellular vesicle trafficking, independently of expression changes in the regulators *tfeb*, *tfe3b*, and *tfec*.

Disruption of chemotactic signaling increases lysosomal staining and microbicidal capacity of macrophages

To assess whether altered expression of vesicle trafficking and lysosomal genes impacts lysosomal function, we assessed the microbicidal capacity of macrophages in *cxcr3.2* mutant and WT embryos. We had previously shown that *cxcr3.2* mutant zebrafish embryos had increased resistance to *Mycobacterium marinum*, a mycobacterium species widely used to model tuberculosis infection (Torraca et al., 2015; Ramakrishnan 2013; Ramakrishnan 2012). However, we did not address the competency of single macrophages in eliminating mycobacteria. Therefore, we infected *cxcr3.2* mutant and WT embryos with the *ΔERP* mutant *M. marinum* strain. This strain lacks the *ERP* (exported repetitive protein) virulence factor that confers resistance to acidity and allows mycobacteria to replicate inside phagolysosomes (Cosma et al., 2006). In zebrafish, the response of macrophages toward *ΔERP M. marinum* has been shown to serve as an indicator of microbicidal efficacy because one can track the clearance of a stationary bacterial population by enumerating the number of bacteria in individual macrophages (Sommer et al., 2020; Clay et al., 2008; Takaki et al., 2013). Data show that *cxcr3.2* mutants cleared *ΔERP M. marinum* infection more efficiently than did WT controls, as they developed fewer bacterial clusters per fish (Figure 2A) and these clusters consisted of lower numbers of bacteria per macrophage (Figure 2B). To assess whether enhanced clearance of bacteria in *cxcr3.2* mutants was related to a higher phagolysosome and lysosome acidity, we injected pH-rodo *E. coli* bioparticles into the circulation of WT and *cxcr3.2* mutant larvae. The pH-rodo *E. coli* bioparticles fluoresce at low pH values, and fluorescence intensity increases with acidity. In line with the RNA-seq data and augmented microbicidal efficacy, phagosomes of *cxcr3.2* mutant macrophages were more acidic at 30–40 min post-injection (mpi) than WT (Figures 2C–2E). To assess whether upregulation of lysosomal genes affected the quantity of lysosomal vesicles within macrophages, we bath-exposed WT and *cxcr3.2* mutant embryos to the intravital LysoTracker dye and quantified the fluorescently stained area within single macrophages. Lysosomal staining was more abundant in *cxcr3.2* mutants than in WT (Figures 2F–2H). These *in vivo* experiments support that upregulation of lysosomal genes in *cxcr3.2* mutants affects both the properties and the total area of lysosomal vesicles and acidic compartments, rendering mutant macrophages more microbicidal.

Tfec inhibition phenocopies increased resistance of *cxcr3.2* mutants to mycobacterial infection, while *tfec* overexpression counteracts enhanced bacterial clearance

Having linked the *cxcr3.2* mutant phenotype to increased lysosomal staining and enhanced bacterial clearing, we asked whether this phenotype could be evoked by manipulating one of the lysosomal regulators. We chose Tfec for this purpose because well-characterized molecular tools are available to modulate its function (Mahony et al., 2016). First, we used a dominant-negative version of Tfec (DN-*tfec*), which has been shown to inhibit the function of endogenous Tfec through competition for Tfec target sites, as DN-*tfec* contains only the DNA-binding domain (Mahony et al., 2016). We injected mRNA encoding *DN-tfec* at the one-cell stage to achieve ubiquitous expression and found *M. marinum* infection of larvae expressing DN-*tfec* to result in a lower bacterial burden than in controls (Figures 3A and 3B; Figure S1A). In contrast, when *tfec* was overexpressed by injecting a cytomegalovirus (CMV) promoter construct driving ubiquitous Tfec expression (CMV:*tfec*), larvae had a higher bacterial burden than did controls (Figures 3C and 3D; Figure S1B). We asked whether *tfec* expression changes upon *M. marinum* infection, but qPCR analyses showed that *M. marinum* infection does not alter *tfec* transcription (Figure S1C). Furthermore, we verified that Tfec inhibition or *tfec* overexpression did not affect expression levels of *cxcr3.2* (Figures S1D and S1E). To confirm whether *tfec* directly affects lysosomal function in macrophages, we inhibited Tfec with the DN-*tfec* construct in *ΔERP M. marinum*-infected larvae and observed that they developed fewer and smaller bacterial clusters than did controls (Figures 3E and 3F). We then used the CMV:*tfec* construct to overexpress *tfec* in *cxcr3.2* mutants and the results showed that it counteracts enhanced bacterial clearance of *cxcr3.2* mutants. In fact, *tfec* overexpression in the *cxcr3.2* mutants restored the bacterial numbers to a level comparable to WT, while non-injected *cxcr3.2* mutants preserved

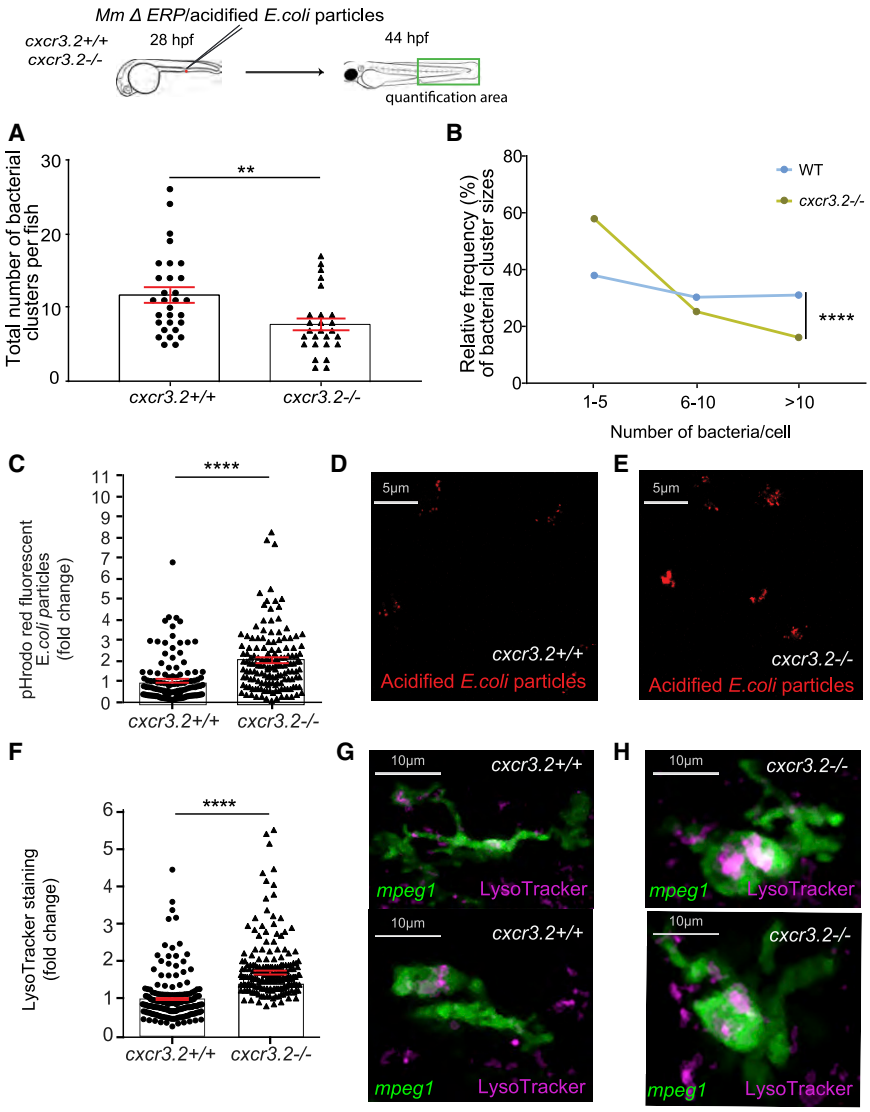

Figure 2. Upregulation of lysosomal genes in *cxcr3.2* mutants is linked with increased microbicidal activity of macrophages

(A and B) Quantification of *M. marinum ΔERP* bacterial clusters in the indicated area showed that infected *cxcr3.2* mutants develop fewer bacterial clusters (A) and that *cxcr3.2* mutants had mostly small bacterial clusters (1–5 bacteria) and few large clusters (>10 bacteria) compared to the WT (B).

(C–E) Normalized intensity of pH-rodo *E. coli* bioparticle clusters in *cxcr3.2* mutants (*cxcr3.2*$^{-/-}$) was higher than in WT larvae (*cxcr3.2*+/+) based on fluorescence quantification (C). Data are expressed as fold change with the average fluorescence intensity in the WT set to 1. Representative confocal images show pH-rodo staining in WT (D) and *cxcr3.2* mutant (E).

(F–H) Normalized data of LysoTracker staining showed that macrophages (*mpeg1:mCherry-F*-positive) in *cxcr3.2* mutants (*cxcr3.2*$^{-/-}$) had higher lysosomal staining than in WT larvae (*cxcr3.2*$^{+/+}$) based on fluorescence quantification (F). Data are expressed as fold change with the average fluorescence intensity in the WT set to 1. Representative images are still confocal images of live WT (G) or *cxcr3.2* mutant (H) macrophages (shown in green) with LysoTracker staining (shown in pink).

A Mann-Whitney test was used to analyze the total number of bacterial clusters per fish of pooled data of two independent replicates of 12–15 fish each (A, C, and F), and a Kolmogorov-Smirnov test was used to analyze the distribution of bacterial cluster sizes (B). All data are shown as mean ± SEM (**$p \leq 0.01$, ****$p \leq 0.0001$).

their enhanced microbicidal capacity, showing a lower total number of bacterial clusters and a lower number of clusters larger than 10 bacteria in size (Figures 3G and 3H). Thus, we showed that manipulating Tfec levels alters the microbicidal capacity of macrophages. In contrast, Tfec overexpression or inhibition did not affect the ability of macrophages to migrate toward a site of injury in WT or *cxcr3.2* mutant larvae (Figures S1F and S1G). Taken together, we conclude that inhibiting Tfec function phenocopies the increased resistance to *M. marinum* of *cxcr3.2* mutants and that increasing Tfec levels counteracts the enhanced microbicidal properties of Cxcr3.2-depleted macrophages.

Disruption of chemotactic signaling in *cxcr3.2* mutant macrophages alters lysosome trafficking and prevents cell polarization during chemotaxis

Chemokine signaling triggers the release of intracellular calcium to orchestrate highly dynamic cell membrane rearrangements that result in a polarized phenotype (Colvin et al., 2010; del Pozo et al., 1995). Lysosome exocytosis delivers layers of lipid membrane to sustain plasma membrane turnover and extension, and it mediates uropod detachment (Colvin et al., 2010; Bretou et al., 2017; Reddy et al., 2001). Therefore, as cells move, lysosomes shuttle between the cell front and rear (Constantin and Laudanna, 2010; Colvin and Luster, 2011). We used lysosomal localization during chemotaxis as an indicator of cell polarization. We stained transgenic (Tg) (*mpeg1:mCherry-F*) *cxcr3.2* mutant and WT larvae with LysoTracker and divided the total macrophage area into halves to calculate the anterior-posterior ratio of LysoTracker staining. WT macrophages had recognizable leading and rear edges and lysosomes moved continuously from rear to the front (1.15:1) during chemotaxis (Figures 4A and 4C). In contrast, the leading edge and uropod of *cxcr3.2* mutant macrophages were not well defined and lysosomes accumulated in the anterior half of the cell (1.74:1) (Figures 4B and 4C). Single cells showed the same trend. The average anteroposterior LysoTracker staining in WT macrophages was 1.13:1 compared with 1.99:1 in *cxcr3.2* mutants (Figures 4D and 4E). Data show that *cxcr3.2* mutant macrophages are not properly polarized and that lysosomes rarely reach the uropod (Figure S2). This vesicle trafficking defect leads to the

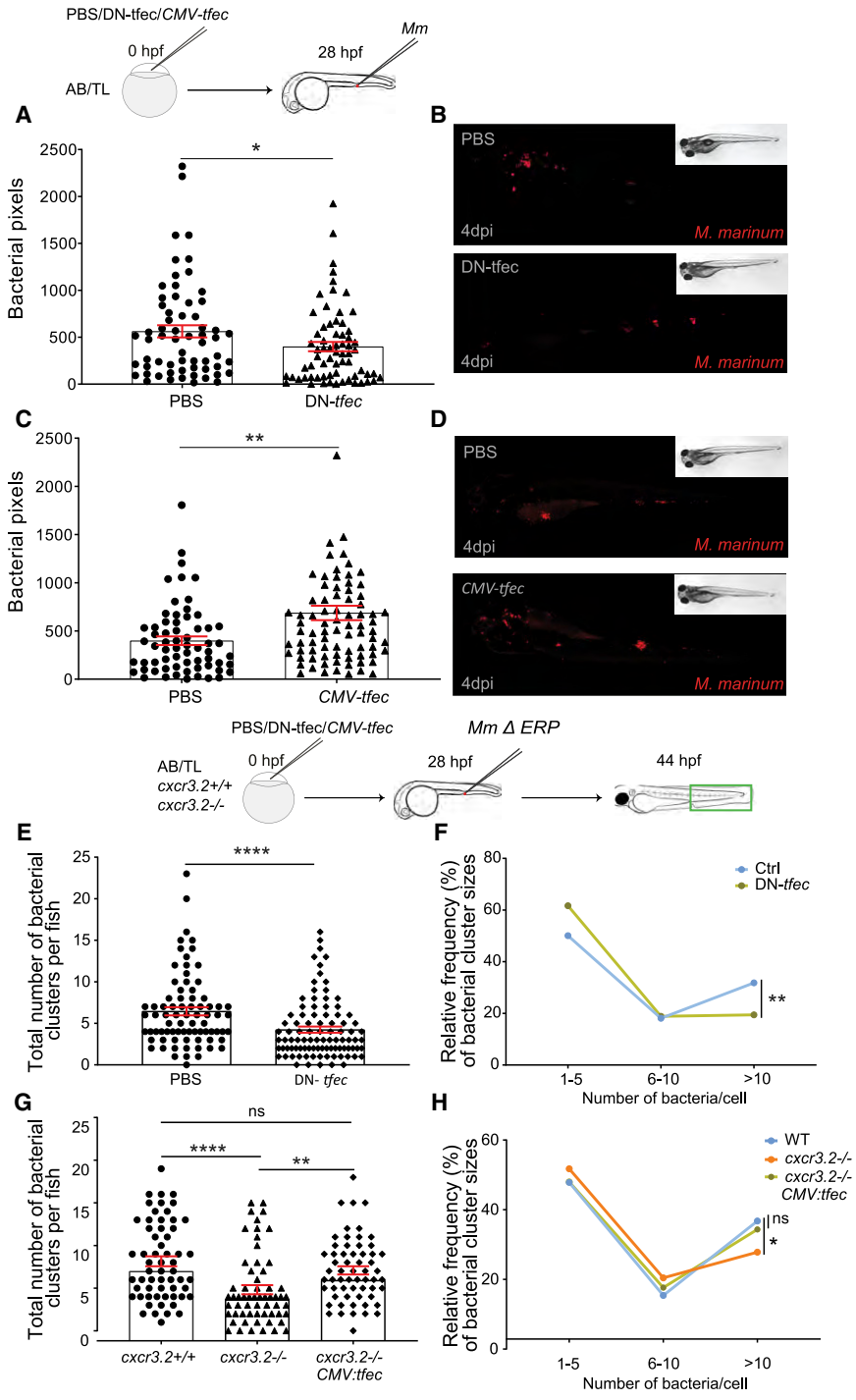

Figure 3.. *tfec* function counteracts enhanced microbicidal capacity of *cxcr3.2* mutants

(A–D) We inhibited Tfec function with the DN-*tfec* construct (A and B) or overexpressed the gene with the *CMV:tfec* construct (C and D) in WT embryos (AB/TL) and subsequently infected them with *M. marinum* mCherry (representative examples are shown). Larvae injected with DN-*tfec* had a lower bacterial burden than did PBS injected controls at 4 days post-infection (dpi) (A and B), while *CMV:tfec* injected larvae had a higher bacterial burden (C and D).

(E and F) *M. marinum ΔERP*-infected WT larvae (AB/TL) previously injected with DN-*tfec* developed fewer (E) and smaller (F) bacterial clusters than did PBS controls and phenocopied *cxcr3.2* mutants in their capacity to clear bacteria.

(G and H) *CMV:tfec*-injected *cxcr3.2* mutants ($cxcr3.2^{-/-}$) infected with *M. marinum ΔERP* lost their enhanced microbicidal capacity and had more (G) and larger (H) bacterial clusters than did WT controls ($cxcr3.2^{+/+}$).

Overall bacterial burden data were analyzed using a two-tailed t test (A–D). Total bacterial clusters per fish were analyzed using a Mann-Whitney test and combined data of three independent replicates of 20–30 larvae (E and G). A Kolmogorov-Smirnov test was used to analyze the distribution of bacterial cluster sizes (F and H). All data are shown as mean ± SEM (*p ≤ 0.05, **p ≤ 0.01, ***p ≤ 0.001 ****p ≤ 0.0001; ns, not significant [p > 0.05]).

accumulation of lysosomes and is tightly linked to aberrant macrophage chemotaxis.

DISCUSSION

Leukocyte chemotaxis is inextricably intertwined with the subcellular localization and exocytosis of lysosomes (Colvin et al., 2010; Bretou et al., 2017; Constantin and Laudanna, 2010; Balasubramani, 2017; Sumoza-Toledo et al., 2011). However, our understanding of the complex network of processes linking chemotaxis and lysosomal function is incomplete. We used the zebrafish model to study the conserved Cxcr3 signaling axis implicated in several inflammatory disorders to show that disrupting Cxcr3 signaling in zebrafish macrophages leads to transcriptional upregulation of lysosomal genes, increased lysosomal staining, enhanced bacterial clearance, altered lysosome trafficking, and aberrant motility. These results provide *in vivo* evidence linking lysosomal function to chemotactic signaling and led us to conclude that disrupting Cxcr3 chemotactic signaling primes macrophages for better clearance of intracellular infection.

We found a marked dysregulation of lysosomal genes in sorted macrophages of larvae lacking Cxcr3.2, the zebrafish homolog of human CXCR3. The expression of lysosomal regulators of the MiTF/TFE protein family remained unaltered, in line with previous work showing that members of this protein family are regulated mostly at the posttranscriptional level (Steingrímsson et al., 2002; Yasumoto and Shibahara, 1997). The induction of lysosomal genes in *cxcr3.2* mutant macrophages

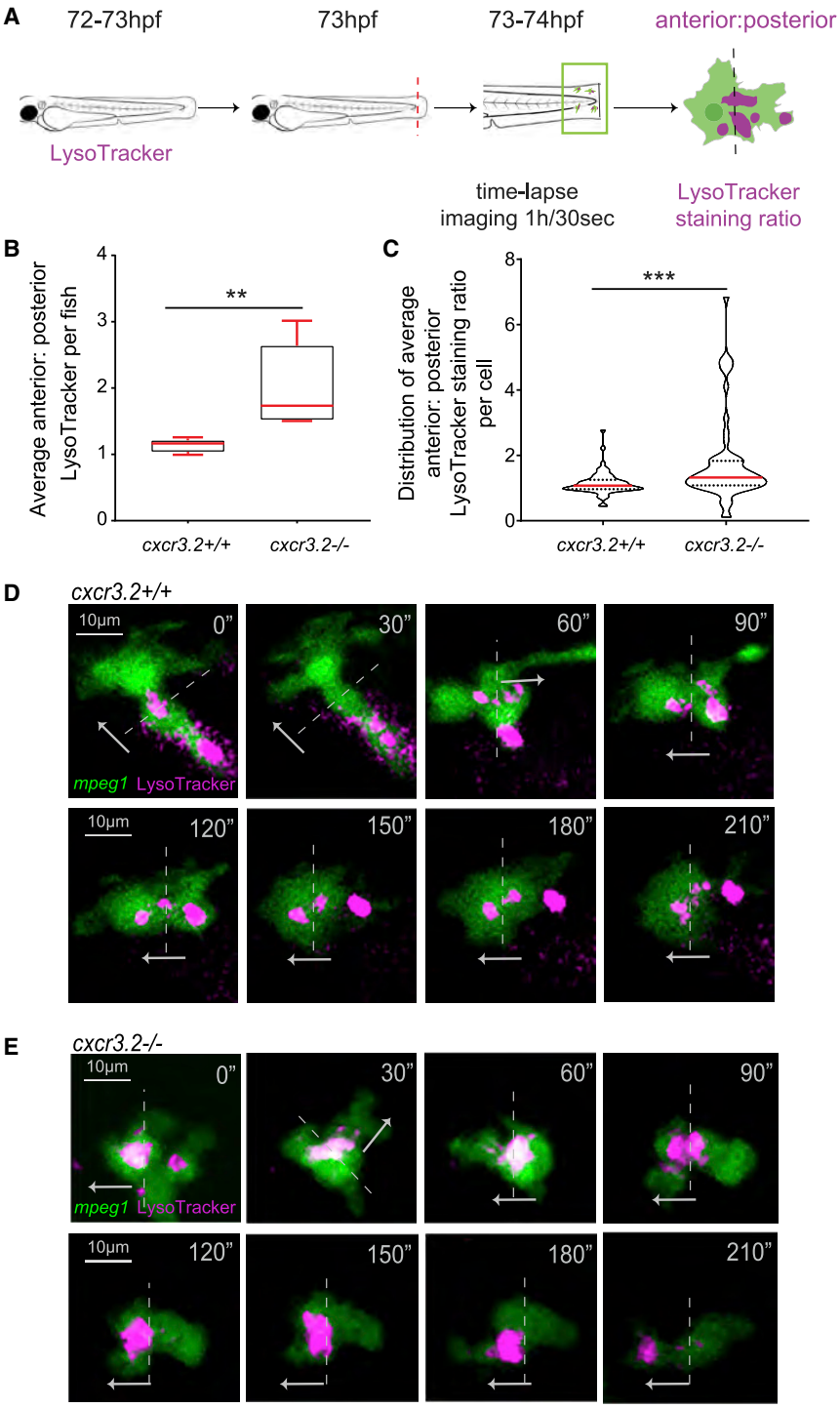

Figure 4. Disruption of Cxcr3.2 signaling in macrophages alters lysosome trafficking and prevents cell polarization during chemotaxis

We assessed lysosome localization during chemotaxis by quantifying the ratio of LysoTracker signal (shown in pink) in the anterior and posterior halves of migrating macrophages (*mpeg1:mCherry-F* labeled, shown in green).

(A) LysoTracker stained Tg(*mpeg1:mCherry-F*) *cxcr3.2* mutant (*cxcr3.2*−/−) and WT larvae (*cxcr3.2*+/+) were time-lapse imaged directly after tail amputation.

(B–E) Data shown in (B) and (C) derive from a total of 63 macrophages in 5 WT larvae (representative images in D) and 57 macrophages in 5 *cxcr3.2* mutant larvae (representative images in E), with at least 7 macrophages analyzed per fish in all cases. Graphs show the average anterior/posterior LysoTracker staining ratio per fish (B) and the average staining ratio per cell (C). Stills at 30-s intervals from representative cells (D and E) and graphs (B and C) show that lysosomes in WT display a small dispersion in the data (B and C) and an even distribution of lysosomes (D), while lysosomes preferentially accumulate in the anterior half in *cxcr3.2* mutant macrophages (E) and show a high variation (B and C). The background of representative images was removed to better show lysosomal distribution in single cells. Dashed lines divide anterior and posterior halves, and arrows indicate the direction of macrophage movement.

Data of anterior/posterior LysoTracker staining per fish were analyzed with a Mann-Whitney test, and data per cell were analyzed using a two-tailed t test. Results are shown as mean ± SEM (**$p \leq 0.01$, ***$p \leq 0.001$).

was linked to increased lysosomal staining, higher phagolysosomal acidity, and enhanced clearance of mycobacteria. A previous work by Shen et al. (2016) used zebrafish to assess lysosomal clearance of apoptotic neuronal debris in RagA (*rraga*) mutant larvae (El-Houjeiri et al., 2019). They reported enlarged lysosomes as in *cxcr3.2* depleted larvae, but low acidity and poor clearance of apoptotic debris as opposed to our observations in *cxcr3.2* mutants. The RagA GTPase anchors TBEB/TFE3 to the lysosomal membrane and interacts with v-ATPases on the lysosomal membrane to acidify the lysosomal lumen (Zoncu et al., 2011; Bar-Peled et al., 2012). The absence of *raga* prevents Tfeb/Tfe3 anchoring and the interaction with v-ATPases, while it promotes the translocation of the transcription factors to the nucleus, arguably leading to sustained *tfeb*-driven induction of lysosomal genes but low intraphagosomal acidity (Shen et al., 2016; Martina and Puertollano, 2013; Dou et al., 2012; Kim et al., 2014). In contrast, the RNA-seq results of *cxcr3.2* mutant macrophages showed induction of genes that could be responsible for highly acidic phagolysosomes, such as the transmembrane amino acid carrier gene *slc361* and the lysosomal v-ATPase subunit c gene *atp6v1c1b*, a direct downstream target of Tfeb (Sardiello et al., 2009). The upregulation of *ctsl.1* (Cathepsin L.1), involved in catabolic processes and the immune response,

could also be linked to enhanced clearance of bacteria in *cxcr3.2* mutant macrophages.

We studied the connection between Cxcr3 chemotactic signaling and lysosomal function by modulating the activity of the lysosomal regulator Tfec and found that blocking Tfec function in WT larvae had a similar host-protective effect as the *cxcr3.2* mutation. Moreover, *tfec* overexpression reverted the protective effect of the *cxcr3.2* mutation and resulted in poor control of bacterial dissemination in WT larvae. It has been shown that lysosome signaling, which involves transcriptional regulators and Ca^{2+} channels, can be triggered by bacterial phagocytosis or macropinocytosis and drives the migration of immune cells besides controlling many other aspects of their function (Bretou et al., 2017; Spix et al., 2020). In our experimental setup, genetic modulations of Tfec activity determined microbicidal activity, but they did not alter wound-induced macrophage migration, indicating that lysosomal activity and the ability to respond to chemotactic cues are not inseparable properties. Nevertheless, these properties could be reciprocally linked. Macrophage migration in *cxcr3.2* mutants might be impaired due to lysosome alterations larger than those inflicted by Tfec alone. Alternatively, increased lysosomal gene expression in *cxcr3.2* mutants could be a result of the motility defect, which is observed even under non-infected conditions due to the production of the Cxcr3.2 ligand (Cxcl11aa) at basal levels as well as at sites of injury or infection (Rougeot et al., 2019; Xie et al., 2019). It has been shown that one of the mammalian TFEC isoforms can strongly inhibit TFE3-mediated gene transactivation (Palmieri et al., 2011; Pastore et al., 2017, 2019). In agreement, we posit that zebrafish Tfec antagonizes the Tfe3-driven transactivation of lysosomal and pro-inflammatory genes and, therefore, inhibiting Tfec function leads to enhanced lysosomal function and pathogen resistance. Altogether, our results support that the highly microbicidal phenotype of *cxcr3.2* mutant macrophages is associated with deregulations in lysosomal function.

Our previous work suggests that the increased microbicidal capacity of *cxcr3.2* mutant macrophages is not the only factor responsible for the infection-resistant phenotype. The macrophage motility defect also contributes, as tissue dissemination of mycobacteria in zebrafish larvae depends on Cxcr3.2-dependent macrophage migration (Torraca et al., 2015; Sommer et al., 2020). The motility defect is the likely cause of the aberrant accumulation pattern of lysosomes during cell migration, which may elicit a transcriptional stress response through the lysosomal regulators, resulting in an increased size of the lysosomal compartment and altered lysosomal properties benefitting host defense. The opposite situation is observed in zebrafish models of lysosomal storage disorders, where the primary defect lies in the deficiency of hydrolytic enzymes, due to which undigested lysosomal material accumulates and disrupts vesicle trafficking and cell migration to the extent that mycobacterial infection cannot be controlled (Berg et al., 2016; Meijer and Aerts, 2016). This is a tight balance, as the outcome of mycobacterial infection is affected positively when macrophage migration is reduced to a limited extent but negatively when macrophage migration is severely impaired (Berg et al., 2016; Meijer and Aerts, 2016; Pagán et al., 2015; Volkman et al., 2010).

By time-lapse imaging we showed that Cxcr3.2-depleted macrophages are not properly polarized during chemotaxis and that lysosomes accumulate in the leading edge of the cell and rarely reach the uropod. The disruption of chemokine signaling axes CXCR4/CXCL12 and CCR2/CCL2 resulted in reduced T cell migration when synaptotagmin SYT7 and the related protein SYTL5 were downregulated (Colvin et al., 2010). Taking these observations as a precedent, the disruption of the Cxcr3 axis might affect intracellular levels and distribution of intracellular chemokine receptor-induced Ca^{2+}, leading to ER stress and lysosome accumulation due to calcineurin-independent Tfeb translocation to the nucleus (Brady et al., 2018a, 2018b). Moreover, vesicle trafficking and lysosome exocytosis might be compromised at low intracellular Ca^{2+} concentrations, further contributing to the accumulation of lysosomes in *cxcr3.2* mutant macrophages and their aberrant motility.

In conclusion, our results in the zebrafish tuberculosis model support that disruption of Cxcr3 chemokine signaling affects intracellular vesicle trafficking in macrophages, preventing them from acquiring a polarized phenotype and migrating toward inflammatory foci while rendering them more microbicidal. It remains to be studied whether altered lysosome function also impacts other leukocytes using the Cxcr3 axis. Especially T cells and neutrophils are of interest in this respect, because altered behavior of these cells has been associated with better control of mycobacterial infection in *cxcr3* mutant mice (Chakravarty et al., 2007; Seiler et al., 2003). Our work contributes to further our understanding of chemotaxis as a complex process that incorporates various physiological processes and integrates different extracellular cues. It emphasizes the importance of vesicle trafficking during chemotaxis and transcriptional and posttranscriptional regulation of lysosome function in immunity. Intravital imaging of zebrafish enabled us to show that there is a direct link between chemokine signaling and lysosomal function that enhances the microbicidal properties and primes macrophages for a better intracellular defense.

STAR★METHODS

Detailed methods are provided in the online version of this paper and include the following:

- KEY RESOURCES TABLE
- RESOURCE AVAILABILITY
  - Lead contact
  - Materials availability
  - Data and code availability
- EXPERIMENTAL MODEL AND SUBJECT DETAILS
  - Ethics statement
  - Zebrafish lines
  - Zebrafish embryo and larva handling
- METHOD DETAILS
  - FACS, RNA extraction, and cDNA synthesis
  - RNA-Seq analysis
  - Quantitative PCR analysis
  - Assessment of microbicidal capacity
  - Acidification assessment using pHrodo
  - LysoTracker staining of acidic compartments

- Systemic infection with *Mycobacterium marinum*
- *tfec* overexpression and Tfec inhibition
- Lysosome localization within macrophages

- QUANTIFICATION AND STATISTICAL ANALYSIS
  - Quantitative PCR analysis
  - RNA-Seq data analysis
  - Assessment of microbicidal capacity
  - Acidification assessment using pH-rodo
  - LysoTracker staining of acidic compartments
  - Systemic infection with *M. marinum*
  - Lysosome localization within macrophages

SUPPLEMENTAL INFORMATION

Supplemental information can be found online at https://doi.org/10.1016/j.celrep.2021.109000.

ACKNOWLEDGMENTS

The authors thank Georges Lutfalla (University of Montpellier) for the macrophage-specific zebrafish reporter lines and Christopher Mahony (University of Birmingham) for the DN-*tfec* constructs, Michiel van der Vaart (Leiden University) for advice on time-lapse imaging, and all members of the fish facility team for zebrafish care. F.S. was supported by a fellowship from CONACYT. V.T. was a Marie Curie Fellow in the Initial Training Network FishForPharma (PITN-GA-2011-289209), funded by the 7th Framework Programme of the European Commission.

AUTHOR CONTRIBUTIONS

F.S. designed and performed experiments, analyzed the data, and wrote the manuscript. V.T. designed and performed experiments and analyzed data. A.E.t.V. and Y.X. contributed to the experimental work. J.W. wrote the script for the "lysosomal distribution" analysis. A.M. supervised the study and reviewed the manuscript. All authors commented on the manuscript and approved the final version.

DECLARATION OF INTERESTS

The authors declare no competing interests.

Received: July 29, 2020
Revised: January 11, 2021
Accepted: March 23, 2021
Published: April 13, 2021

REFERENCES

Adams, K.N., Takaki, K., Connolly, L.E., Wiedenhoft, H., Winglee, K., Humbert, O., Edelstein, P.H., Cosma, C.L., and Ramakrishnan, L. (2011). Drug tolerance in replicating mycobacteria mediated by a macrophage-induced efflux mechanism. Cell *145*, 39–53.

Balasubramani, A. (2017). Lysosomal calcium in dendritic cell migration. Science *358*, 604–605.

Bar-Peled, L., Schweitzer, L.D., Zoncu, R., and Sabatini, D.M. (2012). Ragulator is a GEF for the rag GTPases that signal amino acid levels to mTORC1. Cell *150*, 1196–1208.

Becker, E.L. (1976). Some interrelations of neutrophil chemotaxis, lysosomal enzyme secretion, and phagocytosis as revealed by synthetic peptides. Am. J. Pathol. *85*, 385–394.

Berg, R.D., Levitte, S., O'Sullivan, M.P., O'Leary, S.M., Cambier, C.J., Cameron, J., Takaki, K.K., Moens, C.B., Tobin, D.M., Keane, J., and Ramakrishnan, L. (2016). Lysosomal disorders drive susceptibility to tuberculosis by compromising macrophage migration. Cell *165*, 139–152.

Bernut, A., Herrmann, J.L., Kissa, K., Dubremetz, J.F., Gaillard, J.L., Lutfalla, G., and Kremer, L. (2014). *Mycobacterium abscessus* cording prevents phagocytosis and promotes abscess formation. Proc. Natl. Acad. Sci. USA *111*, E943–E952.

Brady, O.A., Jeong, E., Martina, J.A., Pirooznia, M., Tunc, I., and Puertollano, R. (2018a). The transcription factors TFE3 and TFEB amplify p53 dependent transcriptional programs in response to DNA damage. eLife *7*, e40856.

Brady, O.A., Martina, J.A., and Puertollano, R. (2018b). Emerging roles for TFEB in the immune response and inflammation. Autophagy *14*, 181–189.

Bretou, M., Sáez, P.J., Sanséau, D., Maurin, M., Lankar, D., Chabaud, M., Spampanato, C., Malbec, O., Barbier, L., Muallem, S., et al. (2017). Lysosome signaling controls the migration of dendritic cells. Sci. Immunol. *2*, eaak9573.

Chakravarty, S.D., Xu, J., Lu, B., Gerard, C., Flynn, J., and Chan, J. (2007). The chemokine receptor CXCR3 attenuates the control of chronic *Mycobacterium tuberculosis* infection in BALB/c mice. J. Immunol. *178*, 1723–1735.

Charo, I.F., and Ransohoff, R.M. (2006). The many roles of chemokines and chemokine receptors in inflammation. N. Engl. J. Med. *354*, 610–621.

Chung, M.-C., Kim, H.-K., and Kawamoto, S. (2001). TFEC can function as a transcriptional activator of the nonmuscle myosin II heavy chain-A gene in transfected cells. Biochemistry *40*, 8887–8897.

Clay, H., Volkman, H.E., and Ramakrishnan, L. (2008). Tumor necrosis factor signaling mediates resistance to mycobacteria by inhibiting bacterial growth and macrophage death. Immunity *29*, 283–294.

Colvin, R.A., and Luster, A.D. (2011). Movement within and movement beyond: synaptotagmin-mediated vesicle fusion during chemotaxis. Cell Adhes. Migr. *5*, 56–58.

Colvin, R.A., Means, T.K., Diefenbach, T.J., Moita, L.F., Friday, R.P., Sever, S., Campanella, G.S., Abrazinski, T., Manice, L.A., Moita, C., et al. (2010). Synaptotagmin-mediated vesicle fusion regulates cell migration. Nat. Immunol. *11*, 495–502.

Constantin, G., and Laudanna, C. (2010). Leukocyte chemotaxis: from lysosomes to motility. Nat. Immunol. *11*, 463–464.

Cosma, C.L., Klein, K., Kim, R., Beery, D., and Ramakrishnan, L. (2006). *Mycobacterium marinum* Erp is a virulence determinant required for cell wall integrity and intracellular survival. Infect. Immun. *74*, 3125–3133.

De Duve, C., Pressman, B.C., Gianetto, R., Wattiaux, R., and Appelmans, F. (1955). Tissue fractionation studies. 6. Intracellular distribution patterns of enzymes in rat-liver tissue. Biochem. J. *60*, 604–617.

del Pozo, M.A., Sánchez-Mateos, P., Nieto, M., and Sánchez-Madrid, F. (1995). Chemokines regulate cellular polarization and adhesion receptor redistribution during lymphocyte interaction with endothelium and extracellular matrix. Involvement of cAMP signaling pathway. J. Cell Biol. *131*, 495–508.

Dou, Y., Wu, H.J., Li, H.Q., Qin, S., Wang, Y.E., Li, J., Lou, H.F., Chen, Z., Li, X.M., Luo, Q.M., and Duan, S. (2012). Microglial migration mediated by ATP-induced ATP release from lysosomes. Cell Res. *22*, 1022–1033.

El-Houjeiri, L., Possik, E., Vijayaraghavan, T., Paquette, M., Martina, J.A., Kazan, J.M., Ma, E.H., Jones, R., Blanchette, P., Puertollano, R., and Pause, A. (2019). The transcription factors TFEB and TFE3 link the FLCN-AMPK signaling axis to innate immune response and pathogen resistance. Cell Rep. *26*, 3613–3628.e6.

Flannagan, R.S., Heit, B., and Heinrichs, D.E. (2015). Antimicrobial mechanisms of macrophages and the immune evasion strategies of *Staphylococcus aureus*. Pathogens *4*, 826–868.

Ginhoux, F., Schultze, J.L., Murray, P.J., Ochando, J., and Biswas, S.K. (2016). New insights into the multidimensional concept of macrophage ontogeny, activation and function. Nat. Immunol. *17*, 34–40.

Huang, D.W., Sherman, B.T., Tan, Q., Kir, J., Liu, D., Bryant, D., Guo, Y., Stephens, R., Baseler, M.W., Lane, H.C., and Lempicki, R.A. (2007a). DAVID Bioinformatics Resources: Expanded annotation database and novel algorithms to better extract biology from large gene lists. Nucleic Acids Res. *35*, W169–W175.

Huang, D.W., Sherman, B.T., Tan, Q., Collins, J.R., Alvord, W.G., Roayaei, J., Stephens, R., Baseler, M.W., Lane, H.C., and Lempicki, R.A. (2007b). The

DAVID Gene Functional Classification Tool: A novel biological module-centric algorithm to functionally analyze large gene lists. Genome Biol. *8*, R183.

Kim, Y.C., Park, H.W., Sciarretta, S., Mo, J.S., Jewell, J.L., Russell, R.C., Wu, X., Sadoshima, J., and Guan, K.L. (2014). Rag GTPases are cardioprotective by regulating lysosomal function. Nat. Commun. *5*, 4241.

Lawrence, R.E., and Zoncu, R. (2019). The lysosome as a cellular centre for signalling, metabolism and quality control. Nat. Cell Biol. *21*, 133–142.

Lawson, M.A., and Maxfield, F.R. (1995). Ca^{2+}- and calcineurin-dependent recycling of an integrin to the front of migrating neutrophils. Nature *377*, 75–79.

Li, C.H., and Lee, C.K. (1993). Minimum cross entropy thresholding. Pattern Recognit. *26*, 617–625.

Lister, J.A., Lane, B.M., Nguyen, A., and Lunney, K. (2011). Embryonic expression of zebrafish MiT family genes *tfe3b*, *tfeb*, and *tfec*. Dev. Dyn. *240*, 2529–2538.

Love, M.I., Huber, W., and Anders, S. (2014). Moderated estimation of fold change and dispersion for RNA-seq data with DESeq2. Genome Biol. *15*, 550.

Luzio, J.P., Hackmann, Y., Dieckmann, N.M., and Griffiths, G.M. (2014). The biogenesis of lysosomes and lysosome-related organelles. Cold Spring Harb. Perspect. Biol. *6*, a016840.

Mahony, C.B., Fish, R.J., Pasche, C., and Bertrand, J.Y. (2016). *tfec* controls the hematopoietic stem cell vascular niche during zebrafish embryogenesis. Blood *128*, 1336–1345.

Martina, J.A., and Puertollano, R. (2013). Rag GTPases mediate amino acid-dependent recruitment of TFEB and MITF to lysosomes. J. Cell Biol. *200*, 475–491.

Martina, J.A., Chen, Y., Gucek, M., and Puertollano, R. (2012). MTORC1 functions as a transcriptional regulator of autophagy by preventing nuclear transport of TFEB. Autophagy *8*, 903–914.

Martina, J.A., Diab, H.I., Lishu, L., Jeong-A, L., Patange, S., Raben, N., and Puertollano, R. (2014). The nutrient-responsive transcription factor TFE3 promotes autophagy, lysosomal biogenesis, and clearance of cellular debris. Sci. Signal. *7*, ra9.

Masud, S., Prajsnar, T.K., Torraca, V., Lamers, G.E.M., Benning, M., van der Vaart, M., and Meijer, A.H. (2019). Macrophages target Salmonella by Lc3-associated phagocytosis in a systemic infection model. Autophagy *15*, 796–812.

Medina, D.L., Di Paola, S., Peluso, I., Armani, A., De Stefani, D., Venditti, R., Montefusco, S., Scotto-Rosato, A., Prezioso, C., Forrester, A., et al. (2015). Lysosomal calcium signalling regulates autophagy through calcineurin and TFEB. Nat. Cell Biol. *17*, 288–299.

Meijer, A.H., and Aerts, J.M. (2016). Linking smokers' susceptibility to tuberculosis with lysosomal storage disorders. Dev. Cell *37*, 112–113.

Mi, H., Dong, Q., Muruganujan, A., Gaudet, P., Lewis, S., and Thomas, P.D. (2010). PANTHER version 7: Improved phylogenetic trees, orthologs and collaboration with the Gene Ontology Consortium. Nucleic Acids Res. *38*, D204–D210.

Pagán, A.J., Yang, C.T., Cameron, J., Swaim, L.E., Ellett, F., Lieschke, G.J., and Ramakrishnan, L. (2015). Myeloid growth factors promote resistance to mycobacterial infection by curtailing granuloma necrosis through macrophage replenishment. Cell Host Microbe *18*, 15–26.

Palmieri, M., Impey, S., Kang, H., di Ronza, A., Pelz, C., Sardiello, M., and Ballabio, A. (2011). Characterization of the CLEAR network reveals an integrated control of cellular clearance pathways. Hum. Mol. Genet. *20*, 3852–3866.

Pastore, N., Brady, O.A., Diab, H.I., Martina, J.A., Sun, L., Huynh, T., Lim, J.A., Zare, H., Raben, N., Ballabio, A., and Puertollano, R. (2016). TFEB and TFE3 cooperate in the regulation of the innate immune response in activated macrophages. Autophagy *12*, 1240–1258.

Pastore, N., Vainshtein, A., Klisch, T.J., Armani, A., Huynh, T., Herz, N.J., Polishchuk, E.V., Sandri, M., and Ballabio, A. (2017). TFE3 regulates whole-body energy metabolism in cooperation with TFEB. EMBO Mol. Med. *9*, 605–621.

Pastore, N., Vainshtein, A., Herz, N.J., Huynh, T., Brunetti, L., Klisch, T.J., Mutarelli, M., Annunziata, P., Kinouchi, K., Brunetti-Pierri, N., et al. (2019). Nutrient-sensitive transcription factors TFEB and TFE3 couple autophagy and metabolism to the peripheral clock. EMBO J. *38*, e101347.

Raben, N., and Puertollano, R. (2016). TFEB and TFE3: Linking lysosomes to cellular adaptation to stress. Annu. Rev. Cell Dev. Biol. *32*, 255–278.

Ramakrishnan, L. (2012). Revisiting the role of the granuloma in tuberculosis. Nat. Rev. Immunol. *12*, 352–366.

Ramakrishnan, L. (2013). The zebrafish guide to tuberculosis immunity and treatment. Cold Spring Harb. Symp. Quant. Biol. *78*, 179–192.

Reddy, A., Caler, E.V., and Andrews, N.W. (2001). Plasma membrane repair is mediated by Ca^{2+}-regulated exocytosis of lysosomes. Cell *106*, 157–169.

Reimand, J., Arak, T., Adler, P., Kolberg, L., Reisberg, S., Peterson, H., and Vilo, J. (2016). g:Profiler—A web server for functional interpretation of gene lists (2016 update). Nucleic Acids Res. *44* (*W1*), W83–W89.

Rot, A., and von Andrian, U.H. (2004). Chemokines in innate and adaptive host defense: Basic chemokinese grammar for immune cells. Annu. Rev. Immunol. *22*, 891–928.

Rougeot, J., Zakrzewska, A., Kanwal, Z., Jansen, H.J., Spaink, H.P., and Meijer, A.H. (2014). RNA sequencing of FACS-sorted immune cell populations from zebrafish infection models to identify cell specific responses to intracellular pathogens. Methods Mol. Biol. *1197*, 261–274.

Rougeot, J., Torraca, V., Zakrzewska, A., Kanwal, Z., Jansen, H.J., Sommer, F., Spaink, H.P., and Meijer, A.H. (2019). RNAseq profiling of leukocyte populations in zebrafish larvae reveals a *cxcl11* chemokine gene as a marker of macrophage polarization during mycobacterial infection. Front. Immunol. *10*, 832.

Sachdeva, K., and Sundaramurthy, V. (2020). The interplay of host lysosomes and intracellular pathogens. Front. Cell. Infect. Microbiol. *10*, 595502.

Sardiello, M., Palmieri, M., di Ronza, A., Medina, D.L., Valenza, M., Gennarino, V.A., Di Malta, C., Donaudy, F., Embrione, V., Polishchuk, R.S., et al. (2009). A gene network regulating lysosomal biogenesis and function. Science *325*, 473–477.

Schilling, J.D., Machkovech, H.M., He, L., Diwan, A., and Schaffer, J.E. (2013). TLR4 activation under lipotoxic conditions leads to synergistic macrophage cell death through a TRIF-dependent pathway. J. Immunol. *190*, 1285–1296.

Seiler, P., Aichele, P., Bandermann, S., Hauser, A.E., Lu, B., Gerard, N.P., Gerard, C., Ehlers, S., Mollenkopf, H.J., and Kaufmann, S.H. (2003). Early granuloma formation after aerosol *Mycobacterium tuberculosis* infection is regulated by neutrophils via CXCR3-signaling chemokines. Eur. J. Immunol. *33*, 2676–2686.

Settembre, C., Di Malta, C., Polito, V.A., Garcia Arencibia, M., Vetrini, F., Erdin, S., Erdin, S.U., Huynh, T., Medina, D., Colella, P., et al. (2011). TFEB links autophagy to lysosomal biogenesis. Science *332*, 1429–1433.

Settembre, C., Zoncu, R., Medina, D.L., Vetrini, F., Erdin, S., Erdin, S., Huynh, T., Ferron, M., Karsenty, G., Vellard, M.C., et al. (2012). A lysosome-to-nucleus signalling mechanism senses and regulates the lysosome via mTOR and TFEB. EMBO J. *31*, 1095–1108.

Settembre, C., Fraldi, A., Medina, D.L., and Ballabio, A. (2013). Signals from the lysosome: A control centre for cellular clearance and energy metabolism. Nat. Rev. Mol. Cell Biol. *14*, 283–296.

Shen, K., Sidik, H., and Talbot, W.S. (2016). The Rag-Ragulator complex regulates lysosome function and phagocytic flux in microglia. Cell Rep. *14*, 547–559.

Sherman, B.T., Huang da, W., Tan, Q., Guo, Y., Bour, S., Liu, D., Stephens, R., Baseler, M.W., Lane, H.C., and Lempicki, R.A. (2007). DAVID Knowledgebase: a gene-centered database integrating heterogeneous gene annotation resources to facilitate high-throughput gene functional analysis. BMC Bioinformatics *8*, 426. https://doi.org/10.1186/1471-2105-8-426.

Sommer, F., Torraca, V., Kamel, S.M., Lombardi, A., and Meijer, A.H. (2020). Frontline science: Antagonism between regular and atypical Cxcr3 receptors regulates macrophage migration during infection and injury in zebrafish. J. Leukoc. Biol. *107*, 185–203.

Spix, B., Chao, Y.K., Abrahamian, C., Chen, C.C., and Grimm, C. (2020). TRPML cation channels in inflammation and immunity. Front. Immunol. *11*, 225.

Steingrímsson, E., Tessarollo, L., Pathak, B., Hou, L., Arnheiter, H., Copeland, N.G., and Jenkins, N.A. (2002). Mitf and Tfe3, two members of the Mitf-Tfe family of bHLH-Zip transcription factors, have important but functionally redundant roles in osteoclast development. Proc. Natl. Acad. Sci. USA *99*, 4477–4482.

Stirling, D.R., Suleyman, O., Gil, E., Elks, P.M., Torraca, V., Noursadeghi, M., and Tomlinson, G.S. (2020). Analysis tools to quantify dissemination of pathology in zebrafish larvae. Sci. Rep. *10*, 3149.

Stoop, E.J., Schipper, T., Rosendahl Huber, S.K., Nezhinsky, A.E., Verbeek, F.J., Gurcha, S.S., Besra, G.S., Vandenbroucke-Grauls, C.M., Bitter, W., and van der Sar, A.M. (2011). Zebrafish embryo screen for mycobacterial genes involved in the initiation of granuloma formation reveals a newly identified ESX-1 component. Dis. Model. Mech. *4*, 526–536.

Sumoza-Toledo, A., Lange, I., Cortado, H., Bhagat, H., Mori, Y., Fleig, A., Penner, R., and Partida-Sánchez, S. (2011). Dendritic cell maturation and chemotaxis is regulated by TRPM2-mediated lysosomal Ca^{2+} release. FASEB J. *25*, 3529–3542.

Sung, B.H., Ketova, T., Hoshino, D., Zijlstra, A., and Weaver, A.M. (2015). Directional cell movement through tissues is controlled by exosome secretion. Nat. Commun. *6*, 7164.

Takaki, K., Davis, J.M., Winglee, K., and Ramakrishnan, L. (2013). Evaluation of the pathogenesis and treatment of *Mycobacterium marinum* infection in zebrafish. Nat. Protoc. *8*, 1114–1124.

Tong, Y., and Song, F. (2015). Intracellular calcium signaling regulates autophagy via calcineurin-mediated TFEB dephosphorylation. Autophagy *11*, 1192–1195.

Torraca, V., Cui, C., Boland, R., Bebelman, J.P., van der Sar, A.M., Smit, M.J., Siderius, M., Spaink, H.P., and Meijer, A.H. (2015). The CXCR3-CXCL11 signaling axis mediates macrophage recruitment and dissemination of mycobacterial infection. Dis. Model. Mech. *8*, 253–269.

Tuli, A., and Sharma, M. (2019). How to do business with lysosomes: *Salmonella* leads the way. Curr. Opin. Microbiol. *47*, 1–7.

Upadhyay, S., Mittal, E., and Philips, J.A. (2018). Tuberculosis and the art of macrophage manipulation. Pathog. Dis. *76*, fty037.

van der Sar, A.M., Abdallah, A.M., Sparrius, M., Reinders, E., Vandenbroucke-Grauls, C.M., and Bitter, W. (2004). Mycobacterium marinum strains can be divided into two distinct types based on genetic diversity and virulence. Infect. Immun. *72*, 6306–6312.

van der Vaart, M., Korbee, C.J., Lamers, G.E., Tengeler, A.C., Hosseini, R., Haks, M.C., Ottenhoff, T.H., Spaink, H.P., and Meijer, A.H. (2014). The DNA damage-regulated autophagy modulator DRAM1 links mycobacterial recognition via TLR-MYD88 to autophagic defense [corrected]. Cell Host Microbe *15*, 753–767.

Verastegui, C., Bertolotto, C., Bille, K., Abbe, P., Ortonne, J.P., and Ballotti, R. (2000). TFE3, a transcription factor homologous to microphthalmia, is a potential transcriptional activator of tyrosinase and Tyrpl genes. Mol. Endocrinol. *14*, 449–456.

Visvikis, O., Ihuegbu, N., Labed, S.A., Luhachack, L.G., Alves, A.F., Wollenberg, A.C., Stuart, L.M., Stormo, G.D., and Irazoqui, J.E. (2014). Innate host defense requires TFEB-mediated transcription of cytoprotective and antimicrobial genes. Immunity *40*, 896–909.

Volkman, H.E., Pozos, T.C., Zheng, J., Davis, J.M., Rawls, J.F., and Ramakrishnan, L. (2010). Tuberculous granuloma induction via interaction of a bacterial secreted protein with host epithelium. Science *327*, 466–469.

Xie, Y., Tolmeijer, S., Oskam, J.M., Tonkens, T., Meijer, A.H., and Schaaf, M.J.M. (2019). Glucocorticoids inhibit macrophage differentiation towards a pro-inflammatory phenotype upon wounding without affecting their migration. Dis. Model. Mech. *12*, dmm037887.

Yasumoto, K., and Shibahara, S. (1997). Molecular cloning of cDNA encoding a human TFEC isoform, a newly identified transcriptional regulator. Biochim. Biophys. Acta *1353*, 23–31.

Zhang, R., Varela, M., Forn-Cuní, G., Torraca, V., van der Vaart, M., and Meijer, A.H. (2020). Deficiency in the autophagy modulator Dram1 exacerbates pyroptotic cell death of Mycobacteria-infected macrophages. Cell Death Dis. *11*, 277.

Zhao, G.Q., Zhao, Q., Zhou, X., Mattei, M.G., and de Crombrugghe, B. (1993). TFEC, a basic helix-loop-helix protein, forms heterodimers with TFE3 and inhibits TFE3-dependent transcription activation. Mol. Cell. Biol. *13*, 4505–4512.

Zoncu, R., Bar-Peled, L., Efeyan, A., Wang, S., Sancak, Y., and Sabatini, D.M. (2011). mTORC1 senses lysosomal amino acids through an inside-out mechanism that requires the vacuolar H^+-ATPase. Science *334*, 678–683.

STAR★METHODS

KEY RESOURCES TABLE

REAGENT or RESOURCE	SOURCE	IDENTIFIER
Bacterial and virus strains		
Mycobacterium marinum M-strain: mCherry	van der Sar et al., 2004	N/A
Mycobacterium marinum ΔERP: mWasabi	Takaki et al., 2013	N/A
Critical commercial assays		
miRNeasy mini kit	QIAGEN	217004
SMARTer Universal Low Input RNA Kit for Sequencing	Clontech	634938
iTaq Universal SYBR Green Supermix	BioRad	1725120
LysoTracker Green DND-26	Thermo Fisher Scientific	L7526
pHrodo *E. coli* BioParticles conjugate for phagocytosis	Invitrogen	P35361
Deposited data		
Raw and analyzed RNA sequencing data	This paper	GEO: GSE149942; Data S1, S2, and S3
Experimental models: Organisms/strains		
Zebrafish: AB/TL	ZIRC Zebrafish International Resource Center	ZL1/ZL86
Zebrafish: *Tg(cxcr3.2−/− mpeg1:mCherry-F)*	Torraca et al., 2015; Bernut et al., 2014	ZFIN: u6044/ ump2
Zebrafish: *Tg(cxcr3.2+/+ mpeg1:mCherry-F)*	Torraca et al., 2015; Bernut et al., 2014	ZFIN: u6044/ ump2
Oligonucleotides		
qPCR primers	This paper	Table S1
Recombinant DNA		
DN-*tfec*	Mahony et al., 2016	N/A
pcDNA3.1/V5-His TOPO-*CMV:tfec*	Thermo Fisher Scientific (This paper)	N/A
Software and algorithms		
Java script for "Lysosomal distribution"	This paper	https://sites.imagej.net/Willemsejj/
DESeq2	Love et al., 2014	https://bioconductor.org/packages/release/bioc/html/DESeq2.html
g:profiler	Reimand et al., 2016	https://biit.cs.ut.ee/gprofiler
DAVID bioinformatics tools	Huang et al., 2007a, 2007b; Sherman et al., 2007	https://david.ncifcrf.gov
PANTHER	Mi et al., 2010	http://geneontology.org; http://www.pantherdb.org/

RESOURCE AVAILABILITY

Lead contact

Further information and requests for resources and reagents should be directed to and will be fulfilled by the Lead Contact, Prof. dr. Annemarie H. Meijer (a.h.meijer@biology.leidenuniv.nl).

Materials availability

Plasmids used can be provided by the lead contact.

Data and code availability

Newly generated RNaseq data (Data S1, S2, and S3) are available at the Gene Expression Omnibus database under accession number GSE149942. The Java script for the "Lysosomal distribution" Fiji/ ImageJ plugin can be used following the link: https://sites.imagej.net/Willemsejj/.

EXPERIMENTAL MODEL AND SUBJECT DETAILS

Ethics statement

Zebrafish were handled in compliance with guidelines from the Zebrafish Model Organism Database (http://zfin.org), the EU Animal Protection Directive 2010/63/EU, and the directives of the local animal welfare committee of Leiden University (License number: 10612). All experiments were performed on larval stages before the free feeding stage, which do fall under animal experimentation under EU legislation.

Zebrafish lines

The wt fish line used in this study is AB/TL. The homozygous mutant (*cxcr3.2*−/−) and homozygous wild-type (wt) siblings (*cxcr3.2*+/+) of the *cxcr3.2*^{hu6044} allele were crossed into the Tg(*mpeg1:mCherry-F*)^{ump2} background to visualize macrophages (Bernut et al., 2014; Torraca et al., 2015).

Zebrafish embryo and larva handling

Zebrafish larvae and eggs were stored at 28.5°C in egg water (60 μg/ml Instant Ocean sea salts and 0.0025% methylene blue) and anesthetized with 0.02% buffered tricaine, (3-aminobenzoic acid ethyl ester; Sigma Aldrich, St. Louis, MO, USA) before infections and imaging. Larvae were kept in E2 medium (15 mM NaCl; 0.5 mM KCl, 1.0 mM $MgSO_4$, 150 μM $KH2PO_4$, 50 μM $Na2HPO_4$, 1mM $CaCl_2$; 0.7 mM $NaHCO_3$) for a minimum of 6h prior and during experimental procedures involving pH-rodo and LysoTracker. For confocal imaging, larvae were kept in egg water containing 0.003% PTU (1-phenyl-2-thiourea, Sigma Aldrich) to prevent pigmentation.

METHOD DETAILS

FACS, RNA extraction, and cDNA synthesis

For RNaseq experiments, three biological samples of 150-200 6dpf Tg *(mpeg1:mCherry-F cxcr3.2−/− and cxcr3.2+/+)* larvae were dissociated for FACS following the procedure described in Rougeot et al. (2014). For qPCR analysis on sorted cells, three biological samples of 100-200 Tg *(mpeg1:mCherry-F cxcr3.2−/− and cxcr3.2+/+)* 5dpf larvae were used. For both procedures, RNA was extracted using the miRNeasy mini kit (QIAGEN) according to the manufacturers' instructions. For RNaseq, the synthesis of cDNA was done using the SMARTer Universal Low Input RNA Kit for Sequencing (Clontech) following the manufacturer's guidelines. For qPCR analysis, cDNA was generated using the iScript cDNA Synthesis Kit (Bio-Rad).

RNA-Seq analysis

Illumina RNaseq, mapping and counting of reads was performed as described previously (Rougeot et al., 2019). Analysis of mapped reads was done with the DESeq2 bioinformatics package (https://bioconductor.org/packages/release/bioc/html/DESeq2.html) (Love et al., 2014). Before data processing, lowly expressed genes (< 50 total reads) were filtered. Genes with a p.adj < 0.05 and|log2(-fold change) | > 0.5 cut off were selected for gene ontology analyses (Data S1 and S2). Correspondence between human and zebrafish orthologs was derived through g:profiler (https://biit.cs.ut.ee/gprofiler) and manually curated (Reimand et al., 2016). The significantly affected KEGG pathways were determined by submitting the predicted human orthologs of the significantly regulated zebrafish genes to DAVID bioinformatics tools (https://david.ncifcrf.gov) (Huang et al., 2007a,b; Sherman et al., 2007) (Data S3). The significantly affected Gene Ontology (GO) terms were determined by submitting the predicted human orthologs of the significantly regulated zebrafish genes to PANTHER (Mi et al., 2010). Raw data are deposited in the Gene Expression Omnibus database under accession number GSE149942.

Quantitative PCR analysis

For qPCR analyses on *cxcr3.2* expression, three batches of 10 ABT/TL larvae injected with DN-*tfec*, *CMV:tfec* or PBS each, were collected in QIAzol lysis reagent (QIAGEN). Similarly, 3 batches of infected and non-infected AB/TL larvae were collected to assess *tfec* induction upon infection. Reactions were run on a MyiQ Single-Color Real-Time PCR Detection System (Bio-Rad) using iTaq Universal SYBR Green Supermix (Bio-Rad). Three technical replicates were done for every biological sample. The cycling conditions were: 3 min pre-denaturation at 95°C, 40 denaturation cycles for 15 s at 95°C, annealing for 30 s at 60°C (for all primers), and elongation for 30 s at 72°C. We used the housekeeping gene *ppiab* (peptidylprolyl isomerase Ab) for whole larvae, and *eif5* for sorted macrophages. Primer sequences can be found in Table S1.

Assessment of microbicidal capacity

To determine the microbicidal capacity of zebrafish larval macrophages, embryos were infected with 200 CFU of the attenuated strain, *ΔERP-M. marinum-mWasabi* (Cosma et al., 2006). Larvae were infected in the blood island (BI) with 1nL of a *ΔERP-M. marinum-mWasabi* single-use glycerol stock and microinjected at 28hpf as previously described (Sommer et al., 2020). Infected larvae were fixed with 4% paraformaldehyde (PFA) at 44 hpi, mounted in 1.5% low-melting-point agarose (SphaeroQ, Burgos, Spain) and bacterial clusters were quantified under a Zeiss Observer 6.5.32 laser scanning confocal microscope (Carl Zeiss, Sliedrecht, the Netherlands) using a CApochromat 63x/1.20 W Corr UV-VIR-IR objective (Carl Zeiss, Sliedrecht, the Netherlands).

Acidification assessment using pHrodo

cxcr3.2 mutant and wt larvae were injected with 1 nL of *E. coli* pHrodo *E. coli* BioParticles conjugate for phagocytosis (Invitrogen) at 28-37 hpf into the blood island and imaged over the circulation valley at 30-45 minutes post-injection (mpi). In all cases, the same area was imaged by mounting anesthetized larvae in 1.5% low-melting-point agarose and imaged with Plan-Neofluar 40x/0.9 Imm corr objective on a Zeiss Observer 6.5.32 laser-scanning confocal microscope (Carl Zeiss, Sliedrecht, the Netherlands).

LysoTracker staining of acidic compartments

2-day-old *cxcr3.2* mutant and wt larvae were incubated for 1-2 h with 10 μM LysoTracker Green DND-26 (Invitrogen) in E2 medium. Larvae were anesthetized following the staining and rinsed 3 times for 5 min each with E2 medium and tricaine. Images of live macrophages were acquired with a Plan-Neofluar 40x/0.9 Imm corr objective on a Zeiss Observer 6.5.32 laser-scanning confocal microscope (Carl Zeiss, Sliedrecht, the Netherlands).

Systemic infection with *Mycobacterium marinum*

M. marinum M-strain expressing the fluorescent marker mCherry was grown and prepared freshly for injection as described in Takaki et al. (2013). Embryos were systemically infected with 300CFU of *M. marinum*-mCherry (van der Sar et al., 2004) by microinjection into the blood island at 28hpf. Bacterial burden was quantified based on fluorescence, a well-established approach for assessing mycobacterial infection in zebrafish larvae with advantages over colony forming units determination (Takaki et al., 2013; Adams et al., 2011; Stoop et al., 2011; Stirling et al., 2020). Infected larvae were imaged under a Leica M165C stereo-florescence microscope at 4 days post-infection, and the bacterial burden was determined using a dedicated pixel counting program (Stoop et al., 2011).

tfec overexpression and Tfec inhibition

An expression construct pcDNA3.1/V5-His TOPO-*CMV:tfec* (Mahony et al., 2016) was injected into the yolk at 0 hpf to overexpress the gene in wt and *cxcr3.2* mutant larvae. The CMV promoter is this construct drives ubiquitous expression of transgenes in zebrafish, including expression in uninfected or infected macrophages, relevant to this work (van der Vaart et al., 2014; Zhang et al., 2020; Masud et al., 2019). Overexpression levels were verified by qPCR analysis. Tfec function was inhibited by injecting mRNA encoding DN-*tfec* in wt larvae at 0 hpf to achieve ubiquitous expression in developing embryos. DN-*tfec* mRNA was transcribed from a pCS2+ vector using the SP6 mMachine kit (Ambion) (Mahony et al., 2016). The inhibition of Tfec function by DN-*tfec* was verified through qPCR on *kitlgb*, a downstream target of Tfec (Mahony et al., 2016).

Lysosome localization within macrophages

Time-lapse images of LysoTracker stained macrophages of 3-day-old *cxcr3.2* mutant and wt larvae (5 larvae per genotype) were acquired 1 after tail-amputation every 30 s for 1h. Larvae were mounted in 1.5% low-melting-point agarose and microscopy was done using a Leica TCS SP8 MP confocal microscope (Leica Microsystems). Data were analyzed using a Fiji/ImageJ homemade plugin ''Lysosomal distribution'' (https://sites.imagej.net/Willemsejj/). The plugin divides the total area of single macrophages in half and quantifies the proportion of LysoTracker staining in each part of the cell in every time-frame.

QUANTIFICATION AND STATISTICAL ANALYSIS

Quantitative PCR analysis

The data were analyzed with the 2 $-\Delta\Delta$Ct method. Results are shown as mean ± SEM (ns $p > 0.05$, * $p \leq 0.05$, ** $p \leq 0.01$, *** $p \leq 0.001$). A One-way ANOVA was used to test for significance of the sorted macrophages data and results are plotted as mean ± SEM (ns $p > 0.05$, * $p \leq 0.05$, ** $p \leq 0.01$, *** $p \leq 0.001$). For *cxcr3.2* expression and *tfec* induction on whole larvae, we used a two-tailed t test and plotted the results as mean ± SEM (ns $p > 0.05$, * $p \leq 0.05$, ** $p \leq 0.01$, *** $p \leq 0.001$).

RNA-Seq data analysis

Gene enrichment analysis criteria were Fisher Exact test or False Discovery Rare (FDR) < 0.05 (for DAVID or PANTHER respectively), number of affected genes ≥ 10, fold enrichment ≥ 1.5. The complete data analysis can be found in Data S1, S2, and S3.

Assessment of microbicidal capacity

We used a Mann-Whitney test to analyze the overall bacterial burden of the pooled data of 2 independent replicates of 12-15 fish each, where data are shown as mean ± SEM. A Kolmogorov-Smirnov test was used to analyze the distribution of bacterial cluster sizes (ns $p > 0.05$, * $p \leq 0.05$, ** $p \leq 0.01$, *** $p \leq 0.001$, **** $p \leq 0.0001$).

Acidification assessment using pH-rodo

Fluorescence intensity was assessed using FIJI/ ImageJ quantification tools and data were analyzed using a two-tailed t test. Results are shown as mean ± SEM (ns $p > 0.05$, * $p \leq 0.05$, ** $p \leq 0.01$, *** $p \leq 0.001$, **** $p \leq 0.0001$). Results are expressed as % relative to the wt control (100%).

LysoTracker staining of acidic compartments

To quantify LysoTracker staining within macrophages, the mean intensity of LysoTracker overlapping with *mpeg1:mCherry-F* signal was measured using FIJI/ImageJ quantification tools. Data were analyzed using a two-tailed t test. Results are shown as mean ± SEM (ns $p > 0.05$, * $p \leq 0.05$, ** $p \leq 0.01$, *** $p \leq 0.001$, **** $p \leq 0.0001$). Results are expressed as % relative to the wt control (100%).

Systemic infection with *M. marinum*

Data were analyzed using a two-tailed t test. Results are shown as mean ± SEM (ns $p > 0.05$, * $p \leq 0.05$, ** $p \leq 0.01$, *** $p \leq 0.001$, **** $p \leq 0.0001$) and combined data of 3 independent replicates of 20-30 larvae each.

Lysosome localization within macrophages

The images with labeled macrophages were used to identify the macrophages within the 3D-stack. To reduce background signal for the segmentation the images were blurred using a Gaussian blur with a size of 3 by 3 pixels. Subsequently they were converted to binary images using the Li Thresholding method (Li and Lee, 1993), using a minimum size of 15 pixels. The regions of interest (ROI) obtained over the entire 3D stack were used to analyze the original data, the Gaussian blurred image were only used for segmenting. Each ROI was subsequently split into a top part, and a bottom part by fitting an ellipse over the entire ROI and then splitting it over the short axis. For each ROI in the z stack the intensity at that stack position was measured both in the original macrophage image, as well as in the LysoTracker labeled image. Additionally, the ratio of these intensities was calculated. By analyzing the ROIs separately for each stack position, we made sure there is no overlapping information from cells above or below the cell of interest interfering with our analysis. Finally, the data were organized by cell and by fish and analyzed with a two-tailed t test and a Mann-Whitney test, respectively. Data are shown as mean ± SEM (ns $p > 0.05$, * $p \leq 0.05$, ** $p \leq 0.01$, *** $p \leq 0.001$, **** $p \leq 0.0001$).